HHS Public Access

Author manuscript

Biochemistry. Author manuscript; available in PMC 2018 October 03.

Published in final edited form as:

Biochemistry. 2018 February 06; 57(5): 654–662. doi:10.1021/acs.biochem.7b00999.

Structural features and domain movements controlling substrate binding and cofactor specificity in class II HMG-CoA reductase

Bradley R. Miller and **Yan Kung***

Department of Chemistry, Bryn Mawr College, 101 N. Merion Ave., Bryn Mawr, PA 19010

Abstract

The key mevalonate pathway enzyme 3-hydroxy-3-methylglutaryl coenzyme A (HMG-CoA) reductase (HMGR) uses the cofactor NAD(P)H to reduce HMG-CoA to mevalonate in the production of countless metabolites and natural products. Although HMGR inhibition by statin drugs is well understood, several mechanistic details of HMGR catalysis remain unresolved, and the structural basis for the wide range in cofactor specificity for either NADH or NADPH among HMGRs from different organisms is also unknown. Here, we present crystal structures of HMGR from *Streptococcus pneumoniae* (SpHMGR) alongside kinetic data on the enzyme's cofactor preferences. Our structure of SpHMGR bound with its kinetically preferred NADPH cofactor suggests how NADPH-specific binding and recognition are achieved. In addition, our structure of HMG-CoA-bound SpHMGR reveals large, previously unknown conformational domain movements that may control HMGR substrate binding and enable cofactor exchange without intermediate release during the catalytic cycle. Taken together, this work provides critical new insights into both the HMGR reaction mechanism and the structural basis of cofactor specificity.

Keywords

HMG-CoA reductase; mevalonate pathway; cholesterol; steroid; isoprenoid; X-ray crystallography; protein structure; cofactors

INTRODUCTION

HMGR catalyzes the rate-limiting step of the mevalonate pathway, which is found in all kingdoms of life and is responsible for the biosynthesis of an enormously wide range of molecules, from steroids such as cholesterol to isoprenoids, the largest and most diverse class of natural products. Its key role in the biosynthesis of steroids makes HMGR the target

*Corresponding Author: ykung@brynmawr.edu.

Author Contributions

YK conceived of the project and designed the experiments with BRM, who carried out the kinetic and crystallographic work and solved and refined the X-ray structures. YK and BRM analyzed the data and wrote the paper.

ASSOCIATED CONTENT

Supporting Information

The following files are available free of charge.

Supporting figures that depict electron density following a trial refinement of NADPH in chain C, the interlocking region of the SpHMGR homodimer, and a zoomed-in comparison of the the catalytic histidine position in "closed" and "partially closed" conformations of the C-terminal domain. (PDF)

The authors declare no competing financial interests.

of cholesterol-lowering statin drugs. HMGR performs the four-electron reduction of HMG-CoA to mevalonate and CoA using two equivalents of the redox cofactor NAD(P)H. The enzyme has evolved into two distinct classes,[1–3] where class I HMGRs are present in eukaryotes and in some bacteria and archaea, while class II enzymes are only found in bacteria and archaea. Although both HMGR classes exhibit similar overall folds, with active sites located at a homodimeric interface, there are many significant differences, including those in catalytic regions of the protein.[2]

Class I and class II HMGRs also differ in their NAD(P)H cofactor preferences: although all class I HMGRs including the human enzyme utilize NADPH exclusively, class II HMGRs display a wide range of cofactor specificities. Some class II enzymes use only NADH, including the HMGRs from *Pseudomonas mevalonii* (PmHMGR)[4] and *Burkholderia cenocepacia*,[5] while others use only NADPH, such as HMGR from *Enterococcus faecalis*.[6] Other class II HMGRs are able to use both NADH and NADPH, often with weak or strong preferences for one or the other cofactor, including HMGRs from *Staphylococcus aureus*,[7] *Listeria monocytogenes*,[8] and *Archaeoglobus fulgidus*.[9]

Despite the fact that HMGR inhibition by statins is well understood, the molecular details of the HMGR catalytic mechanism remain somewhat enigmatic.[10] Current proposals suggest that HMG-CoA is first reduced to a mevaldyl-CoA intermediate using the first equivalent of NAD(P)H. The order of the next two steps is uncertain: oxidized $NAD(P)^+$ must be exchanged for a second equivalent of NAD(P)H, and mevaldyl-CoA is also cleaved to form a mevaldehyde intermediate and CoA. Lastly, mevaldehyde is reduced to mevalonate by the second NAD(P)H, and the final products are released.

Interestingly, HMGR can also produce mevalonate if provided with its mevaldyl-CoA or mevaldehyde intermediates,[11, 12] skipping the first reduction step. However, when HMG-CoA is the substrate, neither intermediate is released during the catalytic cycle;[10, 13–15] instead, the enzyme waits until the second reduction step is complete to release the final products. How HMGR is able trigger and accomplish cofactor exchange during the reaction without releasing the bound intermediates is not known. In addition, the structural basis for class II HMGR's wide range of cofactor specificity is also unclear. Greater knowledge of the structural features that control substrate and cofactor binding in class II HMGR would not only provide insight into its catalytic mechanism, it may also enable the development of drugs that target this crucial metabolic enzyme in human pathogens.

To date, crystal structures for only two class II HMGRs have been determined, namely the NADH-specific PmHMGR and HMGR from the major human pathogen *S. pneumoniae* (SpHMGR. SpHMGR inhibition has been previously studied,[16] but its cofactor preferences have not been determined until now. For PmHMGR, many structures are available,[17–19] including the ternary complex depicting the enzyme bound simultaneously with both the cofactor in its oxidized form, NAD^+, and with the substrate HMG-CoA (PDB ID: 1QAX) or the substrate analog dithio-HMG-CoA (PDB ID 4I4B). For SpHMGR, two structures have been determined in the absence of any bound ligands (PDB ID: 3QAE and 3QAU). Interestingly, a C-terminal domain that is disordered in the vast majority of HMGR structures, indicating a high degree of domain mobility, was ordered in structures of the

PmHMGR ternary complex and apo-SpHMGR. Here, the C-terminal domain in apo-SpHMGR was flipped away from the substrate- and cofactor-binding sites, giving rise to an "open" conformation, while the C-terminal domain in the PmHMGR ternary complex was positioned directly over the substrate- and cofactor- binding sites in a "closed" conformation (Figure 1), where the C-terminal domain contributes a catalytically essential histidine, as indicated by mutagenic and structural studies.[18, 20, 21] By alternating between "open" and "closed" conformations, it is possible that the C-terminal domain acts as a "flap" to cover the active site when the substrate and/or cofactor is bound.[18] However, when, how, and what triggers this C-terminal domain movement during the reaction is unknown.

To gain mechanistic insight into HMGR catalysis and to shed light onto how substrate and cofactor binding influence the enzyme's structure during the reaction, we first determined the cofactor preferences of SpHMGR and found that although the enzyme can use both NADH and NADPH to reduce HMG-CoA, it has a strong kinetic preference for NADPH. We also solved two crystal structures of SpHMGR, one bound with substrate HMG-CoA and one bound with its preferred cofactor NADPH, which represents the first structure of an NADPH-bound class II HMGR. These crystal structures not only provide new structural insight into HMGR cofactor binding and specificity, they also reveal new C-terminal domain conformations, allowing us to illuminate the structural movements that enable HMGR reactivity.

MATERIALS AND METHODS

Cloning, expression, and purification.

A codon-optimized, linear *mvaA* gene that encodes SpHMGR (Integrated DNA Technologies) was cloned into a modified pET28b plasmid termed pSKB3, which encodes an N-terminal, TEV-protease-cleavable hexahistidine tag and a kanamycin resistance cassette, using NdeI and BamHI restriction enzymes. The plasmid was transformed into *Escherichia coli* DH10B cells, and its gene sequence was confirmed (Quintara Biosciences) before transformation into BL21(DE3) cells for protein expression.

Cells were grown in lysogeny broth supplemented with kanamycin at 37°C until OD_{600} reached ~0.6. Protein expression was induced with 0.5 mM isopropyl β-D-1-thiogalactopyranoside (IPTG) and proceeded for 18 hours at 16°C. Cells were harvested by centrifugation at 5,000 × *g* for 10 min, flash frozen in liquid nitrogen, and stored at −80°C. Cells were resuspended in lysis buffer (50 mM Tris pH 7.7, 200 mM NaCl, 10% glycerol, 10 mM imidazole) with 0.5 U/μL benzonase (Millipore) and 0.5 mM phenylmethanesulfonyl fluoride (PMSF) and lysed by sonication on ice at 40% amplitude for 9 min with three-second bursts and five-second rests. The lysate was clarified by centrifugation at maximum speed (~37,000 × *g*) for 30 min at 4°C, and the supernatant was applied to a Ni-NTA column equilibrated with lysis buffer. SpHMGR was eluted from the column in fractions using lysis buffer with 300 mM imidazole and assessed for purity by SDS-PAGE. Fractions containing the highest purity were pooled, hexahistidine-tagged TEV protease was added to cleave the hexahistidine tag from SpHMGR, and the sample was dialyzed overnight at 4°C against 50 mM Tris pH 7.7, 200 mM NaCl, 10% glycerol, and 0.5 mM EDTA. The sample was run over a second Ni-NTA column using lysis buffer to purify cleaved SpHMGR. The protein

was further purified by gel filtration on a HiLoad 16/600 Superdex 200 prep grade column (GE Healthcare Life Sciences) equilibrated with 50 mM Tris pH 7.7, 200 mM NaCl, and 10% glycerol using an Akta Pure chromatography system (GE Healthcare Life Sciences). Purified SpHMGR was concentrated to 15 mg/mL, flash frozen dropwise in liquid nitrogen, and stored at −80°C.

Kinetic characterization.

Cofactor specificity was assessed kinetically using a NanoDrop 2000c spectrophotometer (ThermoFisher). Each 100 μL reaction at 37°C contained: 50 mM Tris pH 7.4, 50 mM NaCl, 300 μM HMG-CoA, and NAD(P)H concentrations ranging from 25 μM to 500 μM. Reactions were initiated by the addition of 20 nM SpHMGR for NADPH reactions or 100 nM SpHMGR for NADH reactions. Enzyme-catalyzed oxidation of NAD(P)H was monitored via a decrease in absorbance at 340 nm, using an extinction coefficient of 6,200 M^{-1} cm^{-1}. The Michaelis-Menten constant, K_m, and the maximum velocity, V_{max}, for the production of mevalonate were determined using non-linear regression by fitting the reaction velocities to the Michaelis-Menten equation in GraphPad Prism 6.0. The values for k_{cat} were obtained by dividing V_{max} by the molar enzyme concentration. Values are given as the mean ± the standard error of the mean (SEM) in triplicate experiments.

Crystallization.

Crystallization conditions for HMG-CoA-bound SpHMGR were identified by sparse-matrix screening by sitting-drop vapor diffusion using a Crystal Gryphon (Art Robbins Instruments) with 10 mg/mL SpHMGR plus 1 mM HMG-CoA. Crystals were observed in condition 17 of Crystal Screen 1 (Hampton Research), which contains 100 mM Tris pH 8.5, 200 mM lithium sulfate, and 30% polyethylene glycol (PEG) 4,000. Crystallization conditions were optimized by hanging-drop vapor diffusion with varying lithium sulfate and PEG 4,000 concentrations, and small crystals grew overnight. Crystals were washed in mother liquor, crushed via vortexing, and used as seeds for microseeding. Seeded drops contained 1.0 μL of 10 mg/mL SpHMGR with 1 mM HMG-CoA, 0.8 μL crystallization solution, and 0.2 μL of the seed stock. Large crystals grew in 100 mM Tris pH 8.5, 100–250 mM lithium sulfate, and 15–25% PEG 4,000. The crystals were cryoprotected using the crystallization solution supplemented with 20% glycerol and 1 mM HMG-CoA before flash-cooling in liquid nitrogen.

NADPH-bound SpHMGR crystals grew in the same crystallization condition as the HMG-CoA-bound SpHMGR crystals. However, a new crystal form that took several weeks to grow appeared to use the HMG-CoA-bound SpHMGR microcrystals as nucleation sites for crystal growth. These rod-shaped crystals were optimized using the seeding protocol described above and co-crystallized with 2.5 mM NADPH. Large crystals grew in 100 mM Tris pH 8.5, 100–250 mM lithium sulfate, and 30–40% PEG 4,000. The crystals were cryoprotected using the crystallization solution supplemented with 20% glycerol and 5 mM NADPH before flash-cooling in liquid nitrogen.

X-ray data collection, structure determination, and refinement.

X-ray diffraction data were collected at the Advanced Photon Source (APS) beamline 24-ID-E. The data were indexed, merged, and scaled using iMOSFLM[22] in space group $P1$ with four molecules in the asymmetric unit for the NADPH-bound structure and the space group $P2_1$ with two molecules in the asymmetric unit for the HMG-CoA-bound structure. Structure determination was carried out by molecular replacement using Phaser[23] in the PHENIX suite,[24] where the apo-SpHMGR structure (PDB ID: 3QAE) with unresolved C-terminal domains was used as the search model. Electron density maps indicated that the C-terminal domains were located in novel locations for both structures. Therefore, they were built manually in Coot[25] with iterations of reciprocal space refinement using phenix.refine.[26] After the structures were determined, we noticed that our protein contained a V355E mutational artifact. As this site is quite distant from the cofactor- and substrate-binding sites (>20 Å) as well as the C-terminal domains (>35 Å), we believe that this is unlikely to have a significant impact on the main findings of this paper.

RESULTS

Kinetic characterization of SpHMGR.

Previous studies on SpHMGR focused on enzyme inhibition and characterized the activity using NADPH but did not examine cofactor specificity.[16] To determine the cofactor preference of SpHMGR, we measured steady-state kinetics with varying concentrations of either NADH or NADPH (Table 1). With respect to NADPH, SpHMGR has a K_m of 28.9 ± 5.1 μM and a k_{cat} of 6.85 ± 0.3 s^{-1}. With NADH, the enzyme has a K_m of 153 ± 59.3 μM and a k_{cat} of 0.131 ± 0.02 s^{-1}. The resulting catalytic efficiencies (k_{cat}/K_m) are 2.4×10^5 M^{-1} s^{-1} for NADPH and 8.6×10^2 M^{-1} s^{-1} for NADH. These data show that although SpHMGR can use either cofactor for HMG-CoA reduction, NADPH is the preferred cofactor by approximately 280-fold in terms of k_{cat}/K_m, with both a lower K_m and a higher k_{cat} for NADPH as compared with NADH.

Overall structures.

SpHMGR bound to its preferred cofactor NADPH crystallized in the $P1$ space group with four molecules in the asymmetric unit, arranged as two homodimers (chains A/B and C/D). The overall structure is nearly identical to the prior apo-SpHMGR structures (PDB ID: 3QAE and 3QAU), except for the C-terminal domains, detailed below, with root-mean-square deviation for C_α atoms (rmsd) of 0.23–0.25. Clear electron density was observed for all four monomers of the asymmetric unit, except the C-terminal domains (residues 375–424) of chains A and C were disordered. Electron density in these regions was weak and discontinuous, and thus we did not model the C-terminal domains for chains A and C. Therefore, in the final model chains A and C contain residues 3–372 out of 424, while chains B and D contain residues 11–424 and 3–424, respectively. In addition, positive difference maps showed density in the cofactor binding sites of both chains A and C, representing NADPH binding. For chain A, clear electron density for NADPH was observed, including for the key 2′-phosphate group, though it may be noted that the 2′-phosphate density is partially discontinuous with the rest of the NADPH molecule (Figure 2A), suggesting a small degree of disorder. For chain C, however, electron density for NADPH

was significantly weaker and included significant negative F_O-F_C difference density around the nicotinamide and adenosine rings. A trial refinement at 70% occupancy for NADPH mostly satisfied the difference maps (Figure S1), but because the $2F_O$-F_C maps remained highly discontinuous we chose to leave NADPH in chain C out of the final model.

SpHMGR bound to HMG-CoA crystallized in the $P2_1$ space group with two molecules in the asymmetric unit assembled as a homodimer (chains A and B). The C-terminal domain was resolved only in chain B; therefore, in the final model chain A contains residues 1–379, while chain B contains residues 3–424. Electron density maps showed clear density for HMG-CoA in the substrate-binding sites of both chains (Figure 2B). Complete X-ray diffraction and refinement statistics are found in Table 2.

In the obligate HMGR homodimer, the larger N-terminal domain, which includes the active site, forms the majority of the dimer interface. Interestingly, the interface contains an interlocking motif where residues 1–69 cross and intertwine with each other through loops formed by residues 38–58, forming an interlocked β-sheet that contains several conserved residues and has been observed in prior structures of HMGR (Figure S2A–B).[27, 28] This region is also involved in substrate binding, as in our HMG-CoA bound SpHMGR structure Glu50 and Asn51 from the interlocking loop of one monomer interacts with the adenine ring of HMG-CoA bound by the adjacent monomer (Figure S2C).

Substrate- and cofactor-binding sites.

The HMG-CoA substrate and the NAD(P)H cofactor are both long molecules that bind HMGR with their reactive groups pointing toward each other in the buried active site core at the homodimeric interface and with the rest of the molecules extending out from the active site in different directions, together resembling a “V” shape. Correspondingly, in our structure of HMG-CoA-bound SpHMGR (Figure 3A) the substrate binds with its reactive HMG-moiety in the active site, with Arg257 forming a salt bridge with the carboxylate of the HMG-moiety, which also interacts via a water molecule with the backbone carbonyl of His261 and the side chain of Asn362. The pantothenate group of HMG-CoA then extends out toward the surface of the protein, interacting via water molecules with Gln361 and Ala364. HMG-CoA reaches the protein surface at its diphosphate group, which interacts with Lys380 and Lys384, both from the C-terminal domain. Finally, the adenosine group of HMG-CoA lays down on the surface of the protein, with its adenine ring interacting with the interlocked Glu50 and Asn51 of the opposite monomer, as mentioned above. In addition, the 3′-phosphate of the adenosine ribose forms hydrogen bonds with the backbone NH group of Gly7 as well as the side chain and backbone NH group of Ser9. Interestingly, Ser9 also forms a hydrogen bond with the same Lys384 of the C-terminal domain that interacts with the substrate diphosphate, as described. Though distant in primary sequence, this Ser9-Lys384 interaction thus “bridges” the 3′-phosphate and the diphosphate groups of HMG-CoA. In addition, there are several hydrophobic interactions between the pantothenate and β-mercaptoethylamine moieties of HMG-CoA and the enzyme, including its C-terminal domain.

In our NADPH-bound SpHMGR structure (Figure 3B), only one NADPH molecule is included in the final model. Although the active site lies at the dimer interface, the cofactor

interacts almost exclusively with the opposite monomer as HMG-CoA. As with the substrate, the cofactor binds with its reactive group buried in the active site. Here, the amide group of the nicotinamide ring hydrogen bonds with Asn212, while the 2′-OH group of the nicotinamide's ribose hydrogen bonds with Asp279. From here, the cofactor, like the substrate, extends out toward the protein surface and reaches the solvent at its disphosphate moiety, which interacts directly or through bridging water molecules with the backbone NH groups of Met181, Gly182, Ala183, and Asn184. Together, these four residues form the N-terminal cap of a helix and its preceding loop. The NADPH adenosine group is solvent-exposed, with the adenine ring sandwiched between stacking Lys325 and Arg150 side chains. Intriguingly, Arg150 also forms a salt bridge with the critical 2′-phosphate of NADPH, which also interacts with Ser146 (Figure 3B).

C-terminal domain.

In our NADPH-bound SpHMGR structure, the resolved C-terminal domains of chains B and D are both positioned in "open" conformations, in that they are flipped away from the active site, leaving the substrate- and cofactor-binding sites exposed. However, the C-terminal domains in this structure adopt slightly different "open" conformations from each other (Figure 4A, light and dark orange). Moreover, neither conformation aligns with the previously observed "open" C-terminal domain of the apo-SpHMGR structure (PDB ID: 3QAU) (Figure 4A, blue). These variations in "open" C-terminal domain conformations appear to be caused by interactions with adjacent molecules in the crystal.

On the other hand, the C-terminal domain in our HMG-CoA-bound SpHMGR structure is observed in an entirely new position (Figure 4B). Although flipped more toward the active site relative to the "open" conformations, the C-terminal domain is not positioned over the cofactor-binding site, as was previously observed in the "closed" structures of the PmHMGR ternary complex (Figure 4B). In the "closed" conformation, the C-terminal domain covers both the substrate and the cofactor (Figure 4B, lower panel), while also contacting the N-terminal domain of the adjacent monomer. Instead, the C-terminal domain in our substrate-bound SpHMGR structure is rotated by approximately 90° away from the N-terminal domain of the adjacent monomer and away from the cofactor-binding site as well. In this new position, the C-terminal domain still covers the substrate-binding site; indeed, C-terminal domain residues Lys380 and Lys384 both directly interact with the CoA portion of the substrate (Figures 3A and 5), as described above. Therefore, we term this novel position the "partially closed" conformation of the C-terminal domain, which covers the substrate-binding site while leaving the cofactor-binding site open (Figures 4B and 5). Despite the C-terminal domain maintaining direct contact with the CoA moiety in this "partially closed" conformation, the catalytic histidine (His378 in SpHMGR) is lifted slightly and tilted away from CoA as compared with the "closed" PmHMGR ternary structure (Figure S3).

DISCUSSION

HMGR is a key enzyme in the mevalonate pathway, which is responsible for the biosynthesis of a wide range of molecules, from cholesterol and other steroids to isoprenoid natural products, many of which have medicinal or other uses as commodity chemicals. In

particular, microbial class II HMGRs display a wide range of NAD(P)H cofactor specificities, where some enzymes use either NADH or NADPH exclusively, while others can employ both cofactors to reduce HMG-CoA to mevalonate and CoA. Cofactor usage is a great concern in metabolic engineering for the production of commodity chemicals, including isoprenoid-derived drugs and biofuels,[29, 30] in order to ensure and maintain redox balance and the availability of the correct reductant, either NADH or NADPH. Therefore, a better understanding of the HMGR reaction mechanism and cofactor specificity may lead to the development of HMGR variants whose cofactor preferences are optimized to address issues of redox balance in microorganisms engineered for isoprenoid production via the mevalonate pathway.[31] In addition, greater insight into the reaction mechanism and cofactor preferences of class II HMGR could lead to the development of novel antibiotics, as class II HMGRs are present only in bacteria and archaea. Indeed, the mevalonate pathway has been shown to be essential for growth in many pathogenic microorganisms, including *Streptococcus pneumoniae*, a major cause of pneumonia.[32]

We demonstrate here that class II HMGR from *S. pneumoniae* can utilize both NADPH and NADH, but with a strong preference for NADPH (k_{cat}/K_m of 2.4×10^5 M^{-1} s^{-1} for NADPH versus 8.6×10^2 M^{-1} s^{-1} for NADH). Therefore, we solved the crystal structure of SpHMGR in the presence of NADPH to better understand the structural basis of cofactor specificity, representing the first structure of a class II HMGR bound to NADPH.

In a prior structure of NADH-bound PmHMGR,[18] Asp146 hydrogen-bonds with the NADH adenosine 2′-OH group, presumably preventing the larger and negatively charged 2′-phosphate of NADPH from binding the enzyme. This observation led to possibility that Asp146 confers cofactor specificity in PmHMGR; however, its mutation to alanine, glycine, asparagine, or serine did not switch cofactor preference,[4] as the catalytic efficiency, k_{cat}/K_M, for NADH was still 10–1000-fold greater than for NADPH, indicating that Asp146 in PmHMGR is not solely responsible for cofactor specificity.

Surprisingly, in structures of NADPH-preferring SpHMGR, Asp146 of PmHMGR is not replaced by a smaller or a positively charged residue to accommodate the 2′-phosphate of NADPH, but with a bulky and neutral residue: Tyr144. In fact, we observe that Asp146 of PmHMGR and Tyr144 of SpHMGR are both the first amino acids of a short, seven-residue conserved helix that binds the NAD(P)H cofactor at its adenosine moiety (Figure 6). This helix, which we term the “cofactor-helix”, has a completely different sequence in PmHMGR (residues 146–152) as SpHMGR (residues 144–150): DQLLNSL and YPSIVKR, respectively.

In preferring NADPH over NADH, replacing Asp146 of PmHMGR with the bulkier and uncharged Tyr144 of SpHMGR may at first seem counterintuitive. However, in our cofactor-bound SpHGMR structure Tyr144 prevents the NADPH adenosine ribose from occupying the same space as observed with NADH in PmHMGR (Figure 6). Instead, due to the large size of tyrosine the NADPH adenosine is shifted in the cofactor-binding site compared to NADH in PmHMGR. Though the nicotinamide rings and the diphosphates of NADH and NADPH align well between the PmHMGR and SpHMGR structures, the phosphoribose in SpHMGR is shifted by ~3.0 Å, causing the adenine ring to also be displaced by ~2.0 Å.

Therefore, it appears unlikely that NADPH of SpHMGR could occupy the same space as NADH in PmHMGR, due to the steric hindrance of Tyr144. As a result, Tyr144 blocks phosphoribose from getting close to the start of the cofactor-helix, thus providing space for the 2′-phosphate to interact with Ser146 instead, which is located toward the center of the cofactor-helix. In fact, this serine residue appears to be highly conserved among HMGRs that prefer NADPH, while HMGRs that prefer NADH have a hydrophobic residue in this position (Figure 7), such as Leu148 in PmHMGR. Furthermore, the adenosine ribose of NADPH has shifted enough to allow Arg150 at the end of the SpHMGR cofactor-helix to play a dual role by interacting with both the 2′-phosphate and the adenine ring, as described above. However, in NADH-preferring HMGRs a hydrophobic residue is often found in this position instead of arginine (Figure 7), such as Leu152 in PmHMGR.

Taken together, these structural observations suggest that several residues of the cofactor-helix contribute to NADPH binding and recognition in class II HMGRs. In SpHMGR, the bulky Tyr144 causes a shift in the location of the adenosine moiety of NADPH as compared to NADH in PmHMGR (Figure 6). This shift allows the 2′-phosphate of NADPH to interact with both conserved Ser146 in the center of the cofactor-helix and conserved Arg150 at the end of the helix, which also stacks with the NADPH adenine ring. With these NADPH-binding features now described, future studies to modify this region may offer additional insight into how cofactor specificity may be controlled or engineered.

In addition, our SpHMGR structures reveal large conformational changes upon substrate binding. The C-terminal domain is disordered and absent in most HMGR crystal structures, but has been visualized in the structures of apo-SpHMGR and the ternary PmHMGR complex, bound simultaneously with both cofactor and substrate or substrate analog. These studies indicated that this domain may act as a flexible flap that can open and close over the active site at some point during the reaction.[18] In our NADPH-bound SpHMGR structure, the two resolved C-terminal domains are positioned in “open” conformations that are slightly different from each other (Figure 4A), likely due to crystal packing. This suggests that the C-terminal domain does not occupy a single, rigid “open” conformation, but is flexible and can sample many possible “open” positions that are all distant from the cofactor- and substrate-binding sites. Such flexibility also explains why this domain is often unresolved in HMGR crystal structures. Importantly, these “open” conformations are observed regardless of whether the cofactor is bound, as in our NADPH-bound structure, or unbound, as in the prior apo-SpHMGR structure (PDB ID: 3QAE). Indeed, the partial occupancy for NADPH observed in chain C of our NADPH-bound structure as well as the slightly weaker density for NADPH in chain A are consistent with the notion that these “open” conformations allow for cofactor entry and exit.

Although NADPH-binding alone does not appear to trigger movement of the C-terminal domain to the “closed” conformation, in our substrate-bound SpHMGR structure the C-terminal domain adopts a new, “partially closed” conformation (Figure 4B). This structure represents the first visualization the HMGR C-terminal domain where substrate is bound in the absence of the cofactor. Compared to the fully “closed” conformation depicted in the structures of the PmHMGR ternary complex,[19] the C-terminal domain is rotated ~90° away from the cofactor-binding site and towards the HMG-CoA-binding site (Figure 4B), with

multiple interactions observed between the “partially closed” C-terminal domain and the CoA moiety. Therefore, in this position the cofactor-binding site is left open and accessible, while the substrate-binding site remains closed off by the C-terminal domain (Figures 4B and 5).

The discovery of this “partially closed” conformation might also help to explain how class II HMGRs can undergo cofactor exchange during the reaction cycle without releasing the reaction intermediates mevaldyl-CoA or mevaldehyde, by using a mobile C-terminal domain that adopts multiple conformations (Figure 4C). In this proposed model, before substrate binding the C-terminal domain is “open” and flexible, regardless of whether the cofactor is bound, as described above and observed in the prior apo-SpHMGR structure and the NADPH-bound SpHMGR structure presented here. When both substrate and cofactor are bound, the C-terminal domain closes over both sites and contributes a catalytically essential histidine residue, as seen in structures of the “closed” PmHMGR ternary complex.[18, 19] After the first reduction step that forms $NAD(P)^+$ and the mevaldyl-CoA intermediate, the C-terminal domain rotates away from the cofactor-binding site to the new “partially closed” conformation, which allows for cofactor exchange while keeping the intermediate bound to the enzyme through a number of interactions between the C-terminal domain and the CoA group, as depicted in our HMG-CoA-bound SpHMGR structure. After cofactor exchange is complete and the second NAD(P)H molecule binds, the C-terminal domain can fully close over both cofactor- and substrate-binding sites again, and the second reduction step can proceed. When the reaction is complete, the C-terminal domain can swing open once again to allow for product and cofactor release.

In conclusion, the two crystal structures of SpHMGR described here provide new insight into both the reaction mechanism and the structural basis of cofactor preference in class II HMGR. The crystal structure of NADPH-bound SpHMGR is the first structure of a class II HMGR bound to NADPH, enabling identification and examination of how residues in the “cofactor-helix”, present only in microbial class II enzymes, contribute to NAD(P)H cofactor binding and recognition. This structure also demonstrates the inherent flexibility of the C-terminal domain in the “open” conformation, which is observed regardless of whether the cofactor is bound or not. Meanwhile, the crystal structure of HMG-CoA bound to SpHMGR reveals a new “partially closed” conformation for the C-terminal domain, which suggests how substrate binding may trigger movement of the C-terminal domain from the “open” conformation towards the active site. By covering the substrate-binding site while leaving the cofactor-binding site open, this “partially closed” conformation also illuminates the structural basis for how class II HMGRs can accomplish cofactor exchange during the reaction without the premature and wasteful release of intermediates. With these newly identified conformations of the enzyme, additional studies, including those that investigate intermediate binding in HMGR, may be performed to further probe the conformational landscape of this important enzyme.

Supplementary Material

Refer to Web version on PubMed Central for supplementary material.

ACKNOWLEDGMENT

This work is based upon research conducted at the Northeastern Collaborative Access Team beamlines, which are funded by the National Institute of General Medical Sciences from the National Institutes of Health (P41 GM103403). The Eiger 16M detector on 24-ID-E beam line is funded by a NIH-ORIP HEI grant (S10OD021527). This research used resources of the Advanced Photon Source, a U.S. Department of Energy (DOE) Office of Science User Facility operated for the DOE Office of Science by Argonne National Laboratory under Contract No. DE-AC02–06CH11357.

Funding Sources

This work was supported by the National Institutes of Health (GM116029), Bryn Mawr College, the K/G Fund for Faculty Research, and the Howard Hughes Medical Institute.

ABBREVIATIONS.

HMG-CoA	3-hydroxy-3-methylglutaryl coenzyme A
HMGR	HMG-CoA reductase
PDB	Protein Data Bank
APS	Advanced Photon Source
IPTG	isopropyl β-D-1-thiogalactopyranoside
PMSF	phenylmethanesulfonyl fluoride
NTA	nitrilotriacetic acid
SDS-PAGE	sodium dodecylsulfate-polyacrylamide gel electrophoresis
PEG	polyethylene glycol
rmsd	root-mean-square deviation for C_α atoms

REFERENCES

[1]. Bochar DA, Stauffacher CV, and Rodwell VW (1999) Sequence comparisons reveal two classes of 3-hydroxy-3-methylglutaryl coenzyme A reductase, Mol. Genet. Metab 66, 122–127. [PubMed: 10068515]

[2]. Friesen JA, and Rodwell VW (2004) The 3-hydroxy-3-methylglutaryl coenzyme-A (HMG-CoA) reductases, Genome Biol 5, 248. [PubMed: 15535874]

[3]. Hedl M, Tabernero L, Stauffacher CV, and Rodwell VW (2004) Class II 3-hydroxy-3-methylglutaryl coenzyme A reductases, J. Bacteriol 186, 1927–1932. [PubMed: 15028676]

[4]. Friesen JA, Lawrence CM, Stauffacher CV, and Rodwell VW (1996) Structural determinants of nucleotide coenzyme specificity in the distinctive dinucleotide binding fold of HMG-CoA reductase from *Pseudomonas mevalonii*, Biochemistry 35, 11945–11950. [PubMed: 8810898]

[5]. Schwarz BH, Driver J, Peacock RB, Dembinski HE, Corson MH, Gordon SS, and Watson JM (2014) Kinetic characterization of an oxidative, cooperative HMG-CoA reductase from *Burkholderia cenocepacia*, Biochim. Biophys. Acta 1844, 457–464. [PubMed: 24316250]

[6]. Hedl M, Sutherlin A, Wilding EI, Mazzulla M, McDevitt D, Lane P, Burgner JW, II, Lehnbeuter KR, Stauffacher CV, Gwynn MN, and Rodwell VW (2002) *Enterococcus faecalis* acetoacetyl-coenzyme A thiolase/3-hydroxy-3-methylglutaryl coenzyme A reductase, a dual-function protein of isopentenyl diphosphate biosynthesis, J. Bacteriol 184, 2116–2122. [PubMed: 11914342]

[7]. Wilding EI, Kim DY, Bryant MN, Gwynn RD, Lunsford D, McDevitt JE, Myers JE, Jr., Rosenberg M, Sylvester D, Stauffacher CV, and Rodwell VW (2000) Essentiality, expression, and characterization of the class II 3-hydroxy-3-methylglutaryl coenzyme A reductase of *Staphylococcus aureus*, J. Bacteriol 182, 5147–5152. [PubMed: 10960099]

[8]. Theivagt AE, Amanti EN, Beresford JN, Tabernero L, and Friesen JA (2006) Characterization of an HMG-CoA reductase from *Listeria monocytogenes* that exhibits dual coenzyme specificity, Biochemistry 45, 14397–14406. [PubMed: 17128979]

[9]. Kim D-Y, Stauffacher CV, and Rodwell VW (2000) Dual coenzyme specificity of *Archaeoglobus fulgidus* HMG-CoA reductase, Protein Sci 9, 1226–1234. [PubMed: 10892815]

[10]. Haines BE, Wiest O, and Stauffacher CV (2013) The increasingly complex mechanism of HMG-CoA reductase, Acc. Chem. Res 46, 2416–2426. [PubMed: 23898905]

[11]. Jordan-Starch TC, and Rodwell VW (1989) *Pseudomonas mevalonii* 3-hydroxy-3-methylglutaryl-CoA reductase: Characterization and chemical modification, J. Biol. Chem 264, 17913–17918. [PubMed: 2681185]

[12]. Rétey J, von Stetten E, Coy U, and Lynen F (1970) A probable intermediate in the enzymic reduction of 3-hydroxy-3-methylglutaryl coenzyme A, Eur. J. Biochem 15, 72–76. [PubMed: 4395214]

[13]. Bensch WR, and Rodwell VW (1970) Purification and properties of 3-hydroxy-3-methylglutaryl coenzyme A reductase from *Pseudomonas*, J. Biol. Chem 245, 3755–3762. [PubMed: 4321764]

[14]. Durr IF, and Rudney H (1960) The reduction of β-hydroxy-β-methylglutaryl coenzyme A to mevalonic acid, J. Biol. Chem 235, 2572–2578. [PubMed: 13818862]

[15]. Ferguson JJ, Jr., Durr IF, and Rudney H (1959) The biosynthesis of mevalonic acid, Proc. Natl. Acad. Sci. U.S.A 45, 499–504. [PubMed: 16590405]

[16]. Feng L, Zhou L, Sun Y, Gui J, Wang X, Wu P, Wan J, Ren Y, Qiu S, Wei X, and Li J (2011) Specific inhibitions of annonaceous acetogenins on class II 3-hydroxy-3-methylglutaryl coenzyme A reductase from *Streptococcus pneumoniae*, Bioorg. Med. Chem 19, 3512–3519. [PubMed: 21550257]

[17]. Lawrence CW, Rodwell VW, and Stauffacher CV (1995) Crystal structure of *Pseudomonas mevalonii* HMG-CoA reductase at 3.0 angstrom resolution, Science 268, 1758–1762. [PubMed: 7792601]

[18]. Tabernero L, Bochar DA, Rodwell VW, and Stauffacher CV (1999) Substrate-induced closure of the flap domain in the ternary complex structures provides insights into the mechanism of catalysis by 3-hydroxy-3-methylglutaryl-CoA reductase, Proc. Natl. Acad. Sci. U.S.A 96, 7167–7171. [PubMed: 10377386]

[19]. Steussy CN, Critchelow CJ, Schmidt T, Min J-K, Wrensford LV, Burgner JW, II, Rodwell VW, and Stauffacher CV (2013) A novel role for coenzyme A during hydride transfer in 3-hydroxy-3-methylglutaryl-coenzyme A reductase, Biochemistry 52, 5195–5205. [PubMed: 23802607]

[20]. Darnay BG, Wang Y, and Rodwell VW (1992) Identification of the catalytically important hisitidine of 3-hydroxy-3-methylglutaryl-coenzyme A reductase, J. Biol. Chem 267, 15064–15070. [PubMed: 1634543]

[21]. Darnay BG, and Rodwell VW (1993) His865 is the catalytically important histidyl residue of Syrian hamster 3-hydroxy-3-methylglutaryl-coenzyme A reductase, J. Biol. Chem 268, 8429–8435. [PubMed: 8473286]

[22]. Battye TG, Kontogiannis L, Johnson O, Powell HR, and Leslie AG (2011) iMOSFLM: a new graphical interface for diffraction-image processing with MOSFLM, Acta Cryst. D67, 271–281. [PubMed: 21460445]

[23]. McCoy AJ, Grosse-Kunstleve RW, Adams PD, Winn MD, Storoni LC, and Read RJ (2007) Phaser Crystallographic Software, J. Appl. Cryst 40, 658–674. [PubMed: 19461840]

[24]. Adams PD, Afonine PV, Bunkóczi G, Chen VB, Davis IW, Echols N, Headd JJ, Hung L-W, Kapral GJ, Grosse-Kunstleve RW, McCoy AJ, Moriarty NW, Oeffner R, Read RJ, Richardson DC, Richardson JS, Terwilliger TC, and Zwart PH (2010) PHENIX: a comprehensive Python-based system for macromolecular structure solution, Acta Cryst. D66, 213–221. [PubMed: 20124702]

[25]. Emsley P, and Cowtan K (2004) Coot: model-building tools for molecular graphics, Acta Cryst. D60, 2126–2132. [PubMed: 15572765]

[26]. Afonine PV, Grosse-Kunstleve RW, Echols N, Headd JJ, Moriarty NW, Mustyakimov M, Terwilliger TC, Urzhumtsev A, Zwart PH, and Adams PD (2012) Towards automated crystallographic structure refinement with phenix.refine, Acta Cryst. D68, 352–367. [PubMed: 22505256]

[27]. Istvan ES, Palnitkar M, Buchanan SK, and Deisenhofer J (2000) Crystal structure of the catalytic portion of human HMG-CoA reductase: insights into regulation of activity and catalysis, EMBO J 19, 819–830. [PubMed: 10698924]

[28]. Istvan ES (2001) Bacterial and mammalian HMG-CoA reductase: related enzymes with distinct architectures, Curr. Opin. Struct. Biol 11, 746–751. [PubMed: 11751057]

[29]. Kung Y, Runguphan W, and Keasling JD (2012) From fields to fuels: recent advances in the microbial production of biofuels, ACS Synth Biol 1, 498–513. [PubMed: 23656227]

[30]. George KW, Alonso-Gutierrez J, Keasling JD, and Lee TS (2015) Isoprenoid drugs, biofuels, and chemicals—artemisinin, farnesene, and beyond, Adv. Biochem. Eng. Biotechnol 148, 355–389. [PubMed: 25577395]

[31]. Ma SM, Garcia DE, Redding-Johanson AM, Friedland GD, Chan R, Batth TS, Haliburton JR, Chivian D, Keasling JD, Petzold CJ, Lee TS, and Chhabra SR (2011) Optimization of a heterologous mevalonate pathway through the use of variant HMG-CoA reductases, Metab. Eng 13, 588–597. [PubMed: 21810477]

[32]. Wilding EI, Brown JR, Bryant AP, Chalker AF, Holmes DJ, Ingraham KA, Iordanescu S, So CY, Rosenberg M, and Gwynn MN (2000) Indentificaiton, evolution, and essentiality of the mevalonate pathway for isopentenyl diphosphate biosynthesis in gram-positive cocci, J. Bacteriol 182, 4319–4327. [PubMed: 10894743]

[33]. Liebschner D, Afonine PV, Moriarty NW, Poon BK, Sobolev OV, Terwilliger TC, and Adams PD (2017) Polder maps: improving OMIT maps by excluding bulk solvent, Acta Cryst. D73, 148–157.

[34]. Van Laar TA, Lin Y-H, Miller CL, Karna SLR, Chambers JP, and Seshu J (2012) Effect of levels of acetate on the mevalonate pathway of *Borrelia burgdorferi*, PLoS ONE 7, e38171. [PubMed: 22675445]

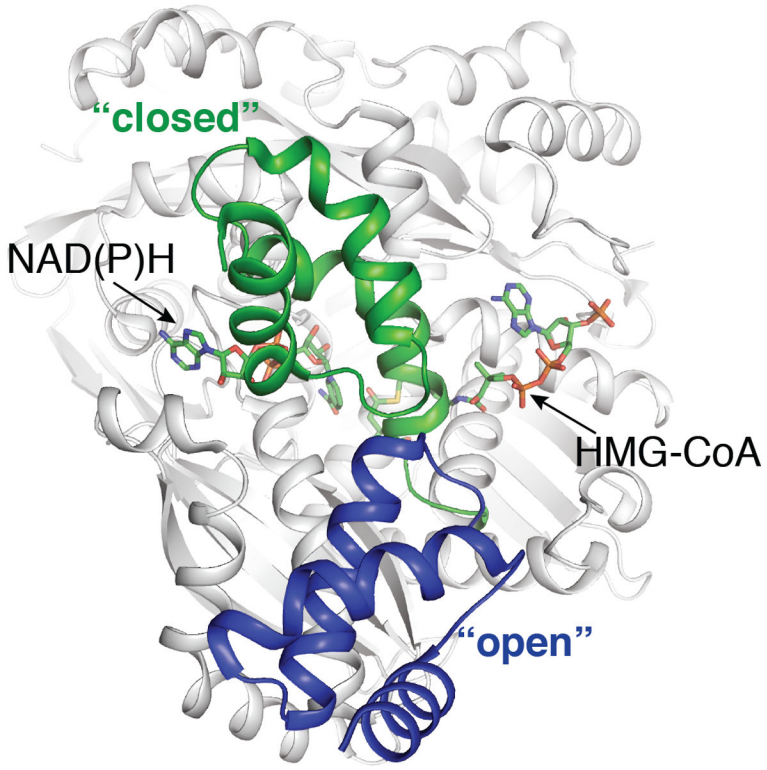

Figure 1.

Structures of “open” and “closed” class II HMGR. Aligned crystal structures of apo-SpHMGR (PDB ID: 3QAU) and the substrate- and cofactor-bound PmHMGR ternary complex (PDB ID: 1QAX), representing “open” (blue) and “closed” (green) conformations of the C-terminal domain (root-mean-square deviation for C_α atoms, rmsd: 0.80). Structures were aligned with their C-terminal domains excluded. Cofactor and substrate are labeled and shown in sticks, with C in green, N in blue, O in red, P in orange, and S in yellow.

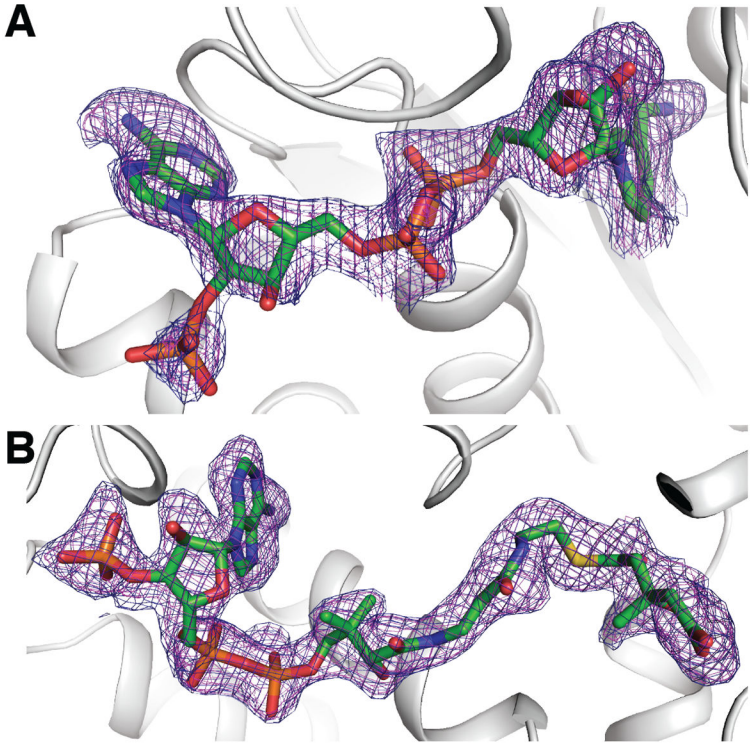

Figure 2.

NADPH and HMG-CoA binding sites of SpHMGR, with mF_O–DF_C omit density for (A) NADPH and (B) HMG-CoA bound to SpHMGR (PDB ID: 5WPJ and 5WPK, respectively). Protein in grey cartoon; NADPH and HMG-CoA in sticks, with C in green, N in blue, O in red, P in orange, and S in yellow; and mF_O–DF_C polder omit map contoured at +3.0 σ (pink mesh) and 2.5 σ (blue mesh) calculated in Phenix.[24, 33]

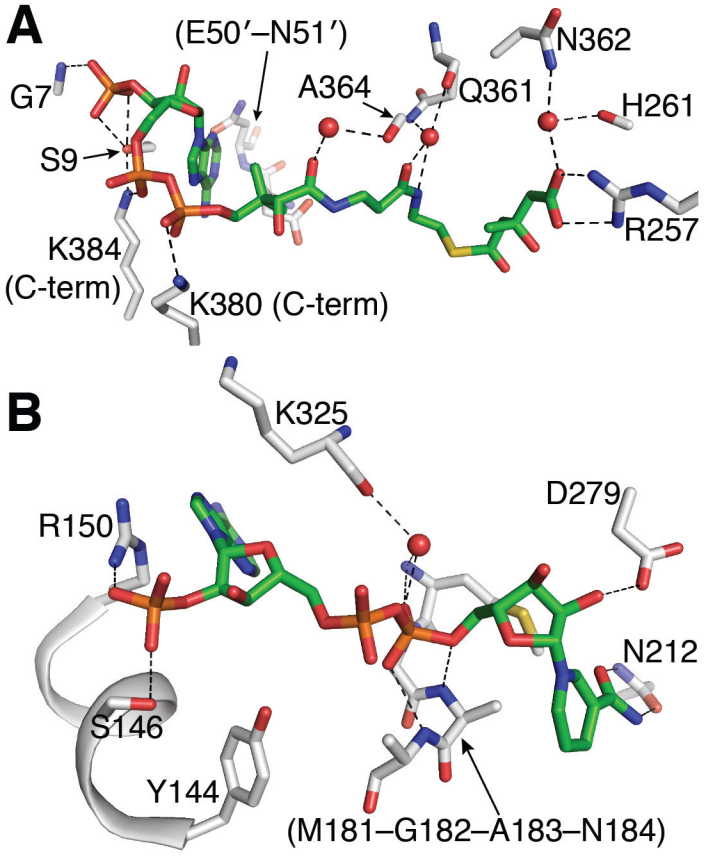

Figure 3.

Interactions between SpHMGR and its substrate and cofactor. (A) The HMG-CoA and (B) NADPH binding sites of SpHMGR. Protein amino acids (C in grey) and all bound ligands (C in green) shown in sticks, with N in blue, O in red, P in orange, and S in yellow, and water shown as spheres. Dashed lines represent hydrogen bonding.

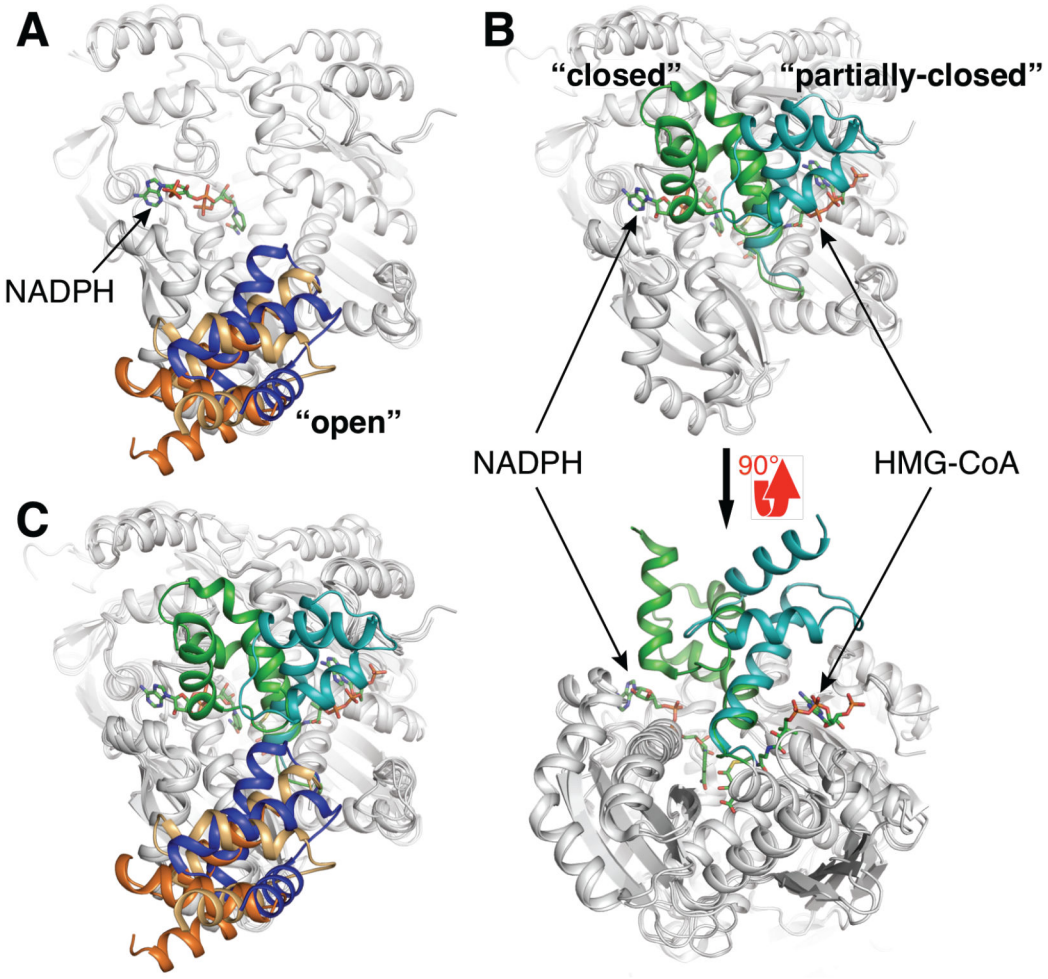

Figure 4.

Conformational movements of the C-terminal domain. (A) Alignment of apo-SpHMGR (PDB ID: 3QAU) with chain B and chain D of the NADPH-bound SpHMGR structure, with C-terminal domains in blue, light orange, and dark orange, respectively (rmsd: 0.23 and 0.25). (B) Alignment of HMG-CoA-bound SpHMGR, C-terminal domain in teal, with the HMG-CoA- and NAD^+-bound PmHMGR ternary complex (PDB ID: 1QAX), C-terminal domain in green (rmsd: 0.89). (C) Overlay of (A) and (B). Proteins shown in grey cartoon, except for C-terminal domains. All ligands shown in sticks, with C in green, N in blue, O in red, P in orange, and S in yellow.

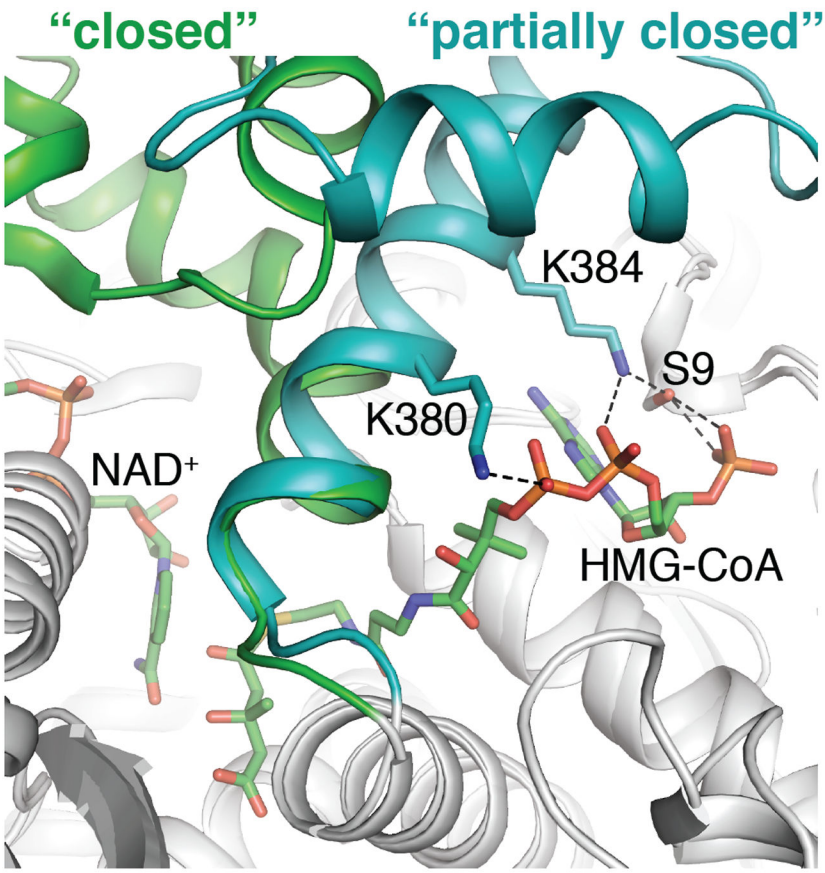

Figure 5.

Zoom-in view of the class II HMGR C-terminal domain in the “closed” conformation in green (from the PmHMGR ternary complex, PDB ID: 1QAX) and the “partially closed” conformation in teal (from the HMG-CoA-bound SpHMGR presented here, PDB ID: 5WPK) from Figure 4B (lower panel). Salt bridge and hydrogen bonding interactions between the “partially closed” C-terminal domain and the HMG-CoA substrate are shown as dashed lines.

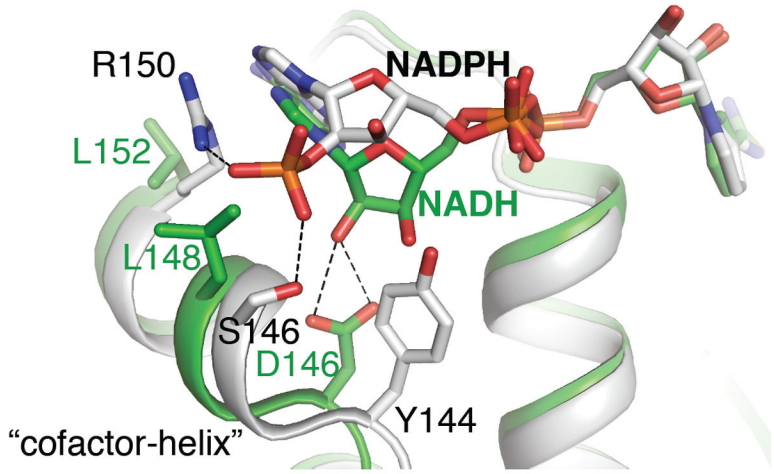

Figure 6.

Comparison of NADH and NADPH cofactor binding sites of class II HMGR. Alignment of the HMG-CoA- and NAD^+-bound PmHMGR ternary complex (green, with residue labels in green) with the NADPH-bound SpHMGR structure (grey, with residue labels in black). The “cofactor-helix” is labeled, and dashed lines represent hydrogen bonding.

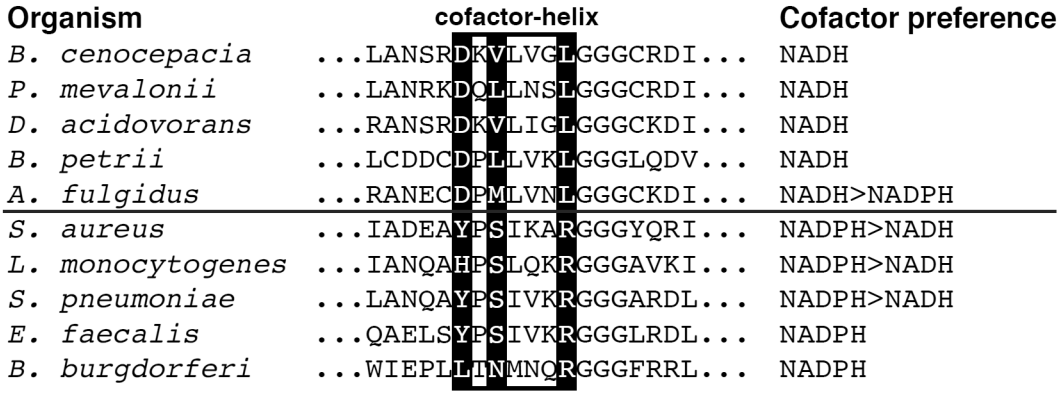

Figure 7.

Sequence alignment of class II HMGRs. Alignment of cofactor-helix sequences (boxed) for class II HMGRs from different organisms is shown alongside known cofactor preferences. NADH-preferring enzymes contain aspartate, a hydrophobic residue, and leucine in the first, third, and final positions of the cofactor-helix, respectively. Meanwhile, in NADPH-preferring enzymes these three positions are occupied by an aromatic or large hydrophobic residue, a small polar residue (often serine), and arginine, respectively. Class II HMGR sequences and preferences are listed as follows: *Burkholderia cenocepacia*,[5] *Pseudomonas mevalonii*,[4] *Delftia acidovorans*,[31] *Bordetella petrii*,[31] *Archaeoglobus fulgidus*,[9] *Staphylococcus aureus*,[7] *Listeria monocytogenes*,[8] *Streptococcus pneumoniae* (this work), *Enterococcus faecalis*,[6] and *Borrelia burgdorferi*.[34]

Table 1.

SpHMGR cofactor preference.

	NADPH	NADH
K_m (μM)	28.9 + 5.1	153 + 59.3
k_{cat} (s^{-1})	6.85 + 0.3	0.131 + 0.02
k_{cat}/K_m (M^{-1} s^{-1})	2.4×10^5	8.6×10^2

Table 2.

Data collection and refinement statistics.

	NADPH-bound SpHMGR	HMG-CoA-bound SpHMGR
PDB ID	5WPJ	5WPK
Diffraction Data		
Beamline	APS, 24-ID-E	APS, 24-ID-E
Wavelength (Å)	0.9792 Å	0.9792 Å
Space group Unit cell	*P*1	*P*21
a, b, c (Å)	58.0, 84.0, 94.2	57.9, 131.2, 57.9
α, β, γ (°)	108.2, 100.6, 109.1	90.0, 102.5, 90.0
Resolution range (Å)[1]	72.72 – 2.00 (2.072–2.00)	19.23–2.30 (2.382–2.30)
Wilson B ($Å^2$)	20.86	23.56
Total reflections	201,205 (20,446)	129,322 (12,606)
Unique reflections	95,302 (9,432)	36,792 (3,643)
Multiplicity	2.1 (2.2)	3.5 (3.5)
Completeness (%)	93.23 (92.35)	98.17 (97.98)
Mean *I/σ(I)*	5.02 (1.88)	6.48 (1.84)
R_{merge}	0.1159 (0.4474)	0.1514 (0.5832)
R_{meas}	0.1556 (0.6014)	0.1788 (0.6913)
CC1/2	0.984 (0.436)	0.987 (0.676)
CC*	0.996 (0.779)	0.997 (0.898)
Refinement		
R_{work}	0.1635 (0.2813)	0.1771 (0.2452)
R_{free}	0.2236 (0.3245)	0.2333 (0.3234)
No. protein/ligand atoms	13,644	6,617
r.m.s.d bonds (Å)	0.008	0.003
r.m.s.d angles (°)	1.243	0.627
Avg. B factor ($Å^2$)	24.0	29.0
Ramachandran analysis		
Favored (%)	97.72	96.87
Allowed (%)	1.90	3.13
Outliers (%)	0.38	0

1. Statistics for the highest-resolution shell are shown in parentheses.